Preliminary Measurement of the J/Ψ Production Cross-section by the South Muon Arm in Run-2.

H. D. Sato, V. Cianciolo

July 10, 2002

1 Introduction

The cross-section for J/Ψ production is simple (in principle) to calculate:

$$\sigma(pp \to J/\Psi) = N_{J/\Psi}/\mathcal{L} \tag{1}$$

Of course, in practice, it is significantly more difficult to extract a correct cross-section than one might guess from this simple formula since $N_{J/\Psi}$ is not the number of J/Ψ that we observe, but rather the number that were actually created — and there are a number of significant correction factors that need to be applied to extract this quantity. The luminosity is also significantly more difficult to accurately compute than is suggested by that one symbol, $\mathcal{L}$.

The equation for $\sigma_{tot}(pp \to J/\Psi \to \mu^+\mu^-)$ (with the correction factors in the chosen factorization) is given by:

$$\sigma_{J/\Psi}^{tot} = \frac{N_{J/\Psi}^{4\pi}}{A\varepsilon_{\mu}^{4\pi} B_{\mu\mu} \varepsilon_{MB}^{J/\Psi}} / \frac{N_{MB}}{\sigma_{tot}^{pp}\varepsilon_{MB}} \tag{2}$$

We have also chosen to calculate the quantities $\frac{d\sigma_{J/\Psi}}{dy}|_{y=1.45}$ and $\frac{d\sigma_{J/\Psi}}{dy}|_{y=1.95}$. These are the values for the differential J/Ψ cross-section observed in the south muon arm's rapidity acceptance (two half-units centered at the indicated values). These quantities have much less systematic error than the total cross-section because we are not integrating over the full (unknown) rapidity distribution of created J/Ψ's; a distribution that is significantly different for two commonly used J/Ψ generators, PYTHIA and the "Ramona Vogt Generator". By observing combining two points in the rapidity distribution from the muon arm measurement with the point at $y = 0$ from the central arm we can significantly reduce our systematic uncertainty on $\sigma_{J/\Psi}^{tot}$.

The equation for this differential cross-section (with the correction factors in the chosen factorization) is given by:

$$\frac{d\sigma_{J/\Psi}}{dy}|_{y^i} = \frac{1}{dy^i} \frac{N_{J/\Psi}^{y^i}}{A\varepsilon_{\mu}^{y^i} B_{\mu\mu} \varepsilon_{MB}^{J/\Psi}} / \frac{N_{MB}}{\sigma_{tot}^{pp}\varepsilon_{MB}} \tag{3}$$

Finally, we will also present a normalized $p_\perp$ spectrum integrated over the full one-unit of the South Muon arm acceptance:

$$\frac{1}{2\pi p_\perp} \frac{d\sigma_{J/\Psi}}{dy dp_\perp}|_{y=1.7,p_\perp^i} = \frac{1}{2\pi p_\perp dp_\perp^i} \frac{N_{J/\Psi}^{y=1.7,p_\perp^i}}{A\varepsilon_{\mu}^{y=1.7,p_\perp^i} B_{\mu\mu} \varepsilon_{MB}^{J/\Psi}} / \frac{N_{MB}}{\sigma_{tot}^{pp}\varepsilon_{MB}} \tag{4}$$

The remainining sections describe the different quantities in this equation, our best estimates for them and the state of our knowledge of systematic errors on each of them.

2 Software

This analysis was performed by first creating reduced versions of the *pp* PRDF files by selecting only those events which passed the MUID blue-logic dimuon (1-Shallow && 1-Deep) trigger [1]. These files were then processed through the third di-muon production pass (as documented on the Run-2 Production page `http://www.phenix.bnl.gov/phenix/WWW/run02/DPM`). V02 MuTR alignment constants were used. These constants has been archived in the database.

ROOT ntuples created from these files were analyzed with ROOT macros. Default reconstruction and pattern recognition parameters (hard-coded in CVS revision 1.15 of `/offline/packages/mui/mMuoRecoModule.C`) were used. All analysis routines and macros can be found in CVS in `offline/analysis/muana` and in the `source` and `macros` subdirectories.

3 $N_{J/\Psi}$

This quantity is simply the number of identified J/Ψ's decaying into muon pairs.

The following cuts were placed on the data set:

- Run Selection — Only runs after the MUID blue-logic trigger was commissioned (37939) were used. In addition, runs between 37939 and 39000 were not used in this analysis because of temporary lack of normalization data (10∼20% of the integrated luminosity after Run 37939). In order to minimize the systematic error due to varying MuTR HV state, only those runs for which the MuTR HV "duty factor" is greater than 0.89 were processed. All such runs are kept, regardless of the number of HV state changes during the run since channels which tripped were automatically restored in a time period much shorter than the length of a typical run. These runs are listed in table 4. A further elimination of runs was made based on examination of the logbook. These bad runs are also listed in table 5 along with reasons for their rejection.
- Online Event Selection — Events were selected by the coincidence of a valid minimum bias (BBC ‖ NTC) trigger and a valid MUID blue logic dimuon trigger (1-Shallow && 1-Deep). Note: there were also MUID blue logic single muon triggers collected during the run, so it may be that there are a few additional J/Ψ's available for a later analysis.
- Vertex Selection — The offline BBC vertex was required to be satisfy ($|z_{vtx}| < 38\,\mathrm{cm}$).
- Single-particle Selection — Valid single particles were required to have GHOSTFLAG == 0.
- Two-particle Selection — To be counted as a J/Ψ candidate (or as background) a pair had to be within $2.5 < M_{inv}(\mathrm{GeV/c}) < 3.7$, and to have consistent reconstructed z vertices for the two particles in the pair ($|z_1^{MUT} - z_2^{MUT}| < 30\,\mathrm{cm}$). z^{MUT} is the z-value at which a track makes its closest approach to the z-axis. Note that no event had more than one J/Ψ.

In addition to counting the number of J/Ψ candidates the number of background pairs also has to be estimated and subtracted. For this analysis the background was determined by simply counting the number of like-sign pairs (of both signs) that pass all of the cuts detailed above. There is an assumption here, beyond the recently much-discussed Poisson requirements on the underlying distributions, which is that there is no charge asymmetry in the detector acceptance. In principle this should be the case for the muon arms, but no attempt has been made to verify the normalization. However, as shown in the mass plots (see figures 1–7), the normalization looks reasonable and in any case the background is small relative to the signal. Figure 2 shows the background subtracted spectrum and the mass and width values. The mass and width look good, although the width is currently a bit worse than expected.

We estimate a systematic error of 10% on the background-subtracted yield based on reasonable adjustments of the mass window. Systematic uncertainties associated with the individual cuts are estimated in the section on acceptance and efficiency. This error is merely the error on our ability to count what's left over after our cuts. Final signal and background counts are given in table 2, below.

4 $A, \varepsilon_{\mu}, \varepsilon_{MB}^{J/\Psi}$

$A\varepsilon_{\mu}\varepsilon_{MB}^{J/\Psi}$ is the product of the acceptance and efficiency of the South Muon arm (triggering and reconstruction/PID) given realistic detector efficiencies. This is quoted as a set of differential $A\varepsilon_{\mu}\varepsilon_{MB}^{J/\Psi}$ values. Approximately 530,000 PYTHIA J/Ψ's (GRVLO94 PDFs; default parameters for polarization, $< K_T >$ and k-factor; direct production only) were generated with a flat vertex distribution ($|z_{vtx}| < 38\,\mathrm{cm}$). 88,000 were found to be within $1.2 < y < 2.2$ and were run through a full PISA simulation of the detector including realistic South Muon arm detector efficiencies, a MuID blue-logic trigger emulator and the BBC performance. $A\varepsilon_{\mu}\varepsilon_{MB}^{J/\Psi}$ is then computed as the fraction of events inside the acceptance bin of interest that fired the simulated BBLL1 trigger (including a 38 cm vertex cut), satisfied the MuID dimuon trigger emulator (1-Deep && 1-Shallow) and which were successfully reconstructed.

MuID panel efficiencies were estimated from a sample of 37 runs in a procedure described in [2]. Using these panel efficiencies the reconstruction efficiencies (data vs. simulation) were in good agreement. The run-to-run variation in the J/Ψ efficiency was determined by reconstructing PYTHIA J/Ψ's in simulations that used the panel efficiencies for the different individual runs. This variation was found to be 11%.

A sample run (39573, HV duty factor = 0.898) was selected to model MuTR dead FEMs, dead electronic channels and dead HV chains. A comparison of the ϕ-dependence of the single particlce MuTR efficiency (simulated vs. real data) was made for this run and is shown in figure 8, below. Good single muons were obtained by demanding tight cuts on reconstructed penetrating MuID roads. There is reasonably good reproduction of the observed efficiencies with the exception of two regions around $\phi = -20°$ to $-40°$ (octant 7), and $\phi = -110°$ to $-160°$ (octant 5). The first problem is apparently due to a simulation bug that is killing a portion of octant 7's ϕ acceptance. The second problem has an unknown origin. Based on MuTR monitor plots (which show relatively low hit occupancy for octant 5) the lower value for data occupancy would appear to be correct. One would expect that 25% of all J/Ψ's would have at least one daughter muon pass through octant 5, and the real efficiency is about 50% of what we're simulating. The discrepency in octant 7 is smaller and of opposite sign, so we assign a systematic error of 10% to the acceptance/efficiency of this particular run based on this disagreement between simulation and data. There is a further systematic error due to run-dependent efficiency that is not taken into account in the simulation. By examining runs at the high and low ends of the HV duty factor range this has been assigned a systematic error of 2%.

Another systematic error comes in because the South Muon arm acceptance has a significant polarization dependence as seen in figure 9 below. This shows the polarization dependence of the acceptance for $J/\Psi's$ (or J/Ψ detection efficiency with the perfect detector) at the peak of the acceptance in y vs. $p_{\perp}$. This dependence is primarily a result of the $p_z < 2\,\mathrm{GeV/c}$ lower-momentum cutoff on daughter muons which cuts off the backwards-going daughter muon in a J/Ψ which decays parallel to its direction of motion. There is no indication in both previous fixed target experiments and Tevatron results that absolute value of the J/Ψ polarization ($|\lambda|$) is larger than 0.3 especailly for low p_T $J/\Psi's$ which dominate our statistics. On the assumption of $|\lambda| < 0.3$, 10% systematic error is assigned.

Finally, we assign a 5% systematic error on the calculation of $\varepsilon_{MB}^{J/\Psi}$ obtained through testing different vertices and different PDFs.

Combining these different errors in quadrature the systematic error on $A\varepsilon_{\mu}\varepsilon_{MB}^{J/\Psi}$ comes to 19%. The statistical error in each bin comes in at 3%. Numbers are shown in table 2, below.

As an aside, we briefly address the significant amount of e-mail discussion over the 4π acceptance of the South Muon arm. In a recent version of the calculation of A_{μ} by itself (the fraction of J/Ψ's that are *reconstructed* in a *perfect detector*) A_{μ} was found to be 1.6%. This was much smaller than the canonical value of 4.1%. The reconciliation is not complete (and perhaps cannot ever be complete). However, the discrepency is not as bad as it looks at first glance. There are a number differences in the calculation, all of which would tend to suppress the original value:

- The old calculation was missing some pieces of obstructing material in the MuTR acceptance.
- The old calculation relied on counting PISA hits in active areas, which are in fact larger than the true sensitive volume.

- On the other hand, the new number explicitly accounts for this by requiring that the J/Ψ be reconstructed - which also factors in track matching, etc.

5 $B_{\mu\mu}$

The particle data book lists the branching ratio for $J/\Psi \to \mu\mu$ as $B_{\mu\mu} = 0.0588 \pm 0.0019$. It is not clear from the PDG, but we have classified this as a systematic error.

6 N_{MB}

This is the number, integrated over all selected runs, of minimum-bias triggered events having offline BBC vertex $|z_{vtx}| < 38\,\text{cm}$. Since the on-line vertex requirement was looser than our requirement the live scalers cannot be used to calculate this number. Instead, the scaled minimum bias triggers are analyzed to determine their vertex distribution. The ratio of events inside the 38 cm cut to the total number of events $\left(\frac{N^{run_i,|z_{vtx}|<38\,\text{cm}}_{MB,\text{prescale}}}{N^{run_i,total}_{MB,\text{prescale}}}\right)$ is determined, run by run, from `spinLumi.root`. This is then used to multiply the number of scaled live bias triggers ($N^{run_i,total}_{MB,\text{live}}$) in each run, which is obtained from the run control logbook due to the discovery of some missing run segments in `spinLumi.root`. It was also discovered that for some runs the reconstructed files had a different number of di-muon triggers then were actually recorded, so a further correction factor was applied. The two correction factors are each of order 5–10% and are of opposite sign, so a 5% systematic error is assigned. The statistical error is negligible.

$$N^{run_i,|z_{vtx}|<38\,\text{cm}}_{MB} = N^{run_i,total}_{MB,\text{live,runcontrol}} \times \frac{N^{run_i,|z_{vtx}|<38\,\text{cm}}_{MB,\text{prescale},\texttt{spinLumi.root}}}{N^{run_i,total}_{MB,\text{prescale},\texttt{spinLumi.root}}} \times \frac{N^{run_i,\text{reconstructed}}_{\text{di-muon}}}{N^{run_i,\text{runcontrol}}_{\text{di-muon}}} \tag{5}$$

$$N_{MB} = \sum_{\text{goodruns}} N^{run_i,|z_{vtx}|<38\,\text{cm}}_{MB} \tag{6}$$

$$= [1.72 \pm 0.09(syst.)] \times 10^9 \tag{7}$$

7 σ^{pp}_{tot}

The total pp cross section at $\sqrt{s} = 200\,\text{GeV}$ has not actually been measured. The PYTHIA value for the inelastic cross-section ($\sigma_{inel} = 42.1\,\text{mb}$) is consistent with the PDG extrapolation from $\sqrt{s} \approx 60\,\text{GeV}$ to $\sqrt{s} \approx 35\,\text{TeV}$. This is the value used in the calculation of ε_{MB} and $\varepsilon^{J/\Psi}_{MB}$ in the next two sections. See the next section for a description of the error on this quantity.

8 ε_{MB}

ε_{MB} is the fraction of inelastic collisions that occur within 38 cm of $z = 0$ which will fire the minimum bias trigger (BBLL1(>1) $\|$ NTC$_w$) and which have their offline BBC $|z_{vtx}|$ reconstructed within 38 cm of $z = 0$. To calculate this the BBC response to the full PYTHIA 42 mb inelastic (including diffractive) cross-section was simulated at different z vertices (the NTC can be ignored since we require an offline BBC vertex). ε_{MB} was found to be 0.51 with relatively little variation found for different z vertices or different PDFs.

The product $\sigma^{pp}_{tot}\varepsilon_{MB}$ has been assigned a 20% error by the luminosity taskforce [3]. We have adopted this value, which is consistent with the approach taken in the $pp \to J/\Psi \to ee$ analysis note [4].

9 Summary

Tables 1 and 2 summarize our current understanding of the values and errors for all quantities that go into calculating the J/Ψ production cross-section in pp collisions at $\sqrt{s} = 200\,\text{GeV/c}$. Substituting these values into equations 3–4, we obtain the final cross-section values, summarized in table 3. Statistical and systematic errors have been independently added in quadrature. Note that sometimes the branching ratio is included, sometimes not.

The final rapidity distribution (incorporating the branching ratio) is shown in figure 10, below. See figure caption for details. The $p_\perp$ distribution is shown in figure 11, below.

References

[1] H. D. Sato, PHENIX Technical Note 395, 2002.

[2] H. D. Sato, PHENIX Technical Note , to be published.

[3] PHENIX Analysis Note , to be published.

[4] PHENIX Analysis Note , to be published.

Quantity	Value	Systematic Error (σ_i^{syst}/i)
$B_{\mu\mu}$	0.06	0.03
N_{MB}	1.72×10^9	0.05
$\sigma_{tot}^{pp}(mb)$	42.1	0.20
ε_{MB}	0.51	0

Table 1: Summary table of common cross-section inputs values and systematic errors. Statistical errors are negligible. Note - the combined systematic error on $\sigma_{tot}^{pp}\varepsilon_{MB}$ is shown on the σ_{tot}^{pp} line.

y, dy, $p_\perp$, $dp_\perp$	Quantity	Value	Statistical Error (σ_i^{stat}/i)	Systematic Error (σ_i^{syst}/i)
1.70, 1.0, all, –	$N_{J/\Psi}$	$41 - 5 = 36$	0.19	0.10
	$A\varepsilon_\mu\varepsilon_{MB}^{J/\Psi}$	0.0121	0.03	0.19
1.45, 0.5, all, –	$N_{J/\Psi}$	$29 - 3 = 26$	0.22	0.10
	$A\varepsilon_\mu\varepsilon_{MB}^{J/\Psi}$	0.0131	0.03	0.19
1.95, 0.5, all, –	$N_{J/\Psi}$	$12 - 2 = 10$	0.37	0.10
	$A\varepsilon_\mu\varepsilon_{MB}^{J/\Psi}$	0.0108	0.03	0.19
1.70, 1.0, 0.5, 1.0	$N_{J/\Psi}$	$12 - 2 = 10$	0.37	0.10
	$A\varepsilon_\mu\varepsilon_{MB}^{J/\Psi}$	0.0140	0.03	0.19
1.70, 1.0, 1.5, 1.0	$N_{J/\Psi}$	$17 - 2 = 15$	0.29	0.10
	$A\varepsilon_\mu\varepsilon_{MB}^{J/\Psi}$	0.0121	0.03	0.19
1.70, 1.0, 2.5, 1.0	$N_{J/\Psi}$	$9 - 1 = 8$	0.40	0.10
	$A\varepsilon_\mu\varepsilon_{MB}^{J/\Psi}$	0.0114	0.03	0.19

Table 2: Summary table of binning-specific cross-section inputs values and errors.

Quantity	Value (nb or nb/(GeV/c)^2)	Statistical Error (σ_i^{stat}/i)	Systematic Error (σ_i^{syst}/i)
$\frac{d\sigma_{J/\Psi}}{dy}\vert_{y=1.7}$	620	0.19	0.29
$\frac{d\sigma_{J/\Psi}}{dy}\vert_{y=1.45}$	820	0.22	0.29
$\frac{d\sigma_{J/\Psi}}{dy}\vert_{y=1.95}$	380	0.37	0.29
$\frac{1}{2\pi p_\perp}\frac{d\sigma_{J/\Psi}}{dydp_\perp}\vert_{y=1.7,p_\perp=0.5}$	47	0.37	0.29
$\frac{1}{2\pi p_\perp}\frac{d\sigma_{J/\Psi}}{dydp_\perp}\vert_{y=1.7,p_\perp=1.5}$	27	0.29	0.29
$\frac{1}{2\pi p_\perp}\frac{d\sigma_{J/\Psi}}{dydp_\perp}\vert_{y=1.7,p_\perp=2.5}$	9.3	0.40	0.29

Table 3: Cross-section summary table.

39000	39002	39003	39084	39085	39089	39090	39091	39092	39094	39095	39096
39097	39098	39099	39100	39101	39102	39104	39105	39106	39107	39108	39109
39340	39341	39342	39343	39345	39346	39347	39348	39349	39350	39351	39358
39362	39364	39365	39367	39370	39371	39373	39374	39445	39446	39450	39451
39453	39455	39460	39461	39566	39567	39568	39570	39572	39573	39575	39576
39579	39580	39636	39639	39640	39642	39643	39644	39647	39713	39715	39716
39717	39718	39719	39720	39722	39724	39725	39726	39727	39728	39731	39732
39734	39735	39736	39737	39740	39743	39767	39769	39770	39772	39774	39778
39780	39782	39785	39792	39870	39875	39877	39879	39881	39883	39884	39895
39898	39899	39900	39963	39966	39967	39968	39969	39970	39971	39972	39973
39974	39978	39979	39980	39982	39984	39986	39989	39990	39991	39992	39993
39994	40082	40083	40084	40085	40086	40087	40088	40089	40090	40091	40092
40117	40122	40124	40127	40129	40130	40132	40133	40135	40136	40139	40141
40142	40143	40144	40145	40146	40147	40204	40206	40208	40210	40211	40213
40216	40217	40218	40219	40220	40222	40223	40224	40227	40228	40288	40289
40290	40291	40292	40293	40296	40300	40304	40305	40306	40307	40309	40311
40312	40321	40322	40374	40376	40377	40378	40379	40381	40454	40457	40458
40461	40462	40463	40563	40564	40565	40566	40567	40569	40570	40571	40573
40574	40633	40635	40636	40637	40638	40639					

Table 4: List of runs after 39000 with MuTR HV duty factor > 0.89.

Reason for rejection	Run Numbers			
Reconstruction unsuccessful	38912	39573	39725	39732
	39960	40091	40092	40135
	40136			
MuTr HV study	39960	40640	40643	40645
	40646	40647	40648	40649
	40650	40651	40653	
Massive MuID/MuTr HV trip	37949			
MuID Glink problem	38985	38986	38987	
Low HV	38988			
Vernier scan	40300			
Beam gas study	40301			
Small N_{event}	39566	39774	39832	39895
	39958	40124	40309	40381
Bad fill (vertex)	40115			

Table 5: List of bad runs.

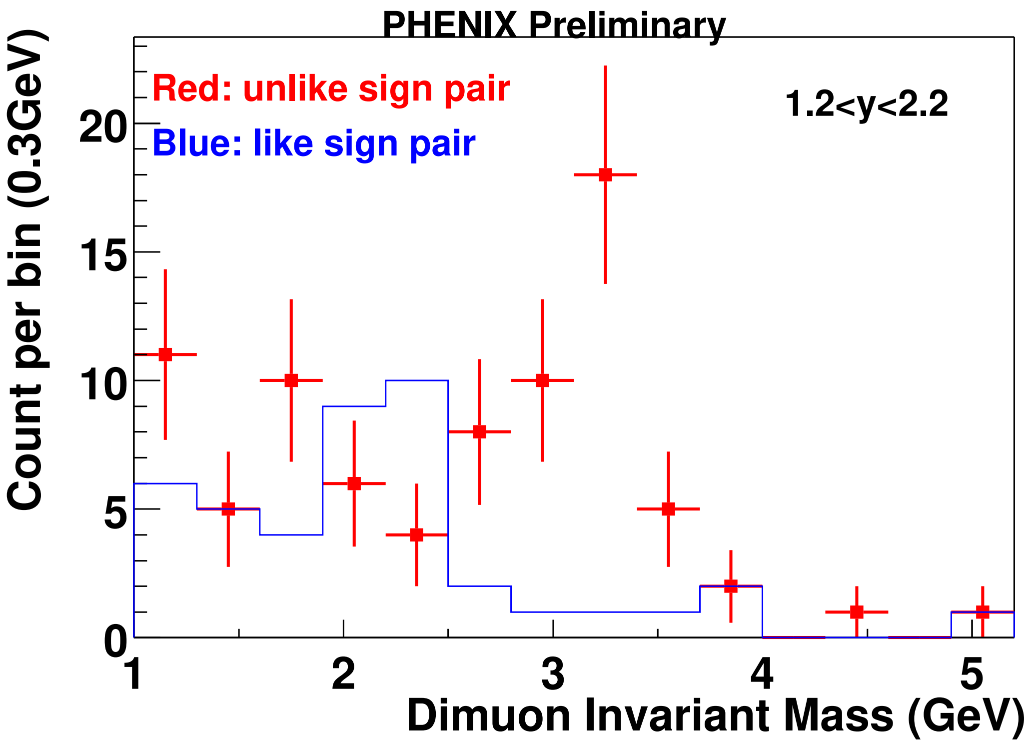

Figure 1: M_{inv} distribution for all dimuons passing cuts described in the text.

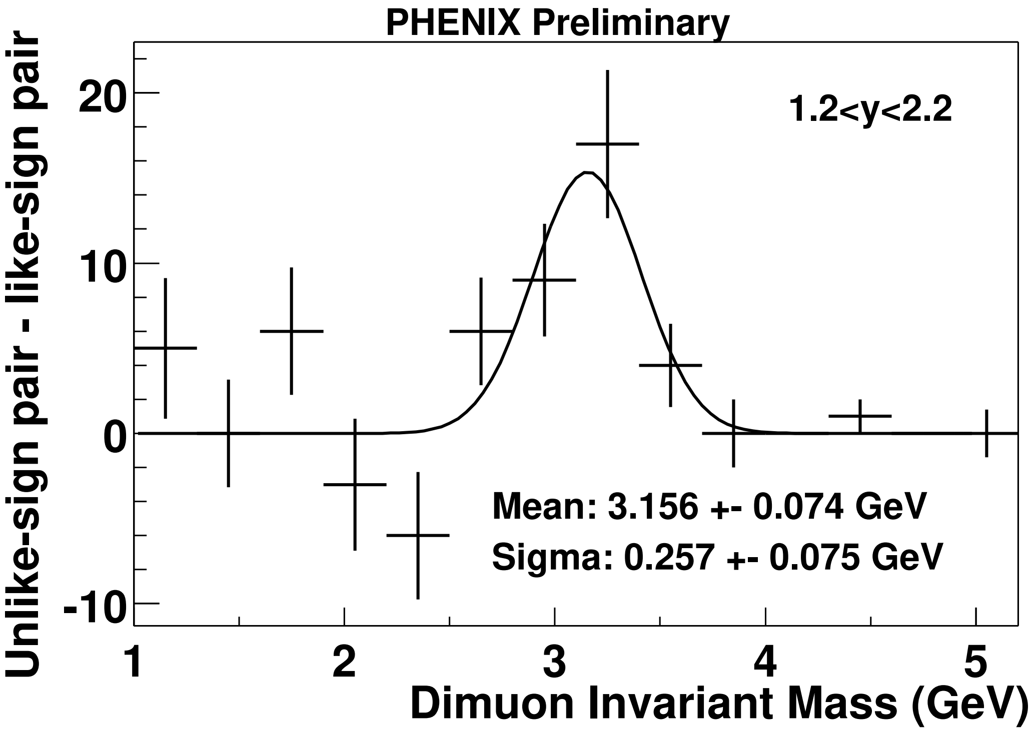

Figure 2: M_{inv} distribution for background subtracted unlike-sign dimuon spectrum.

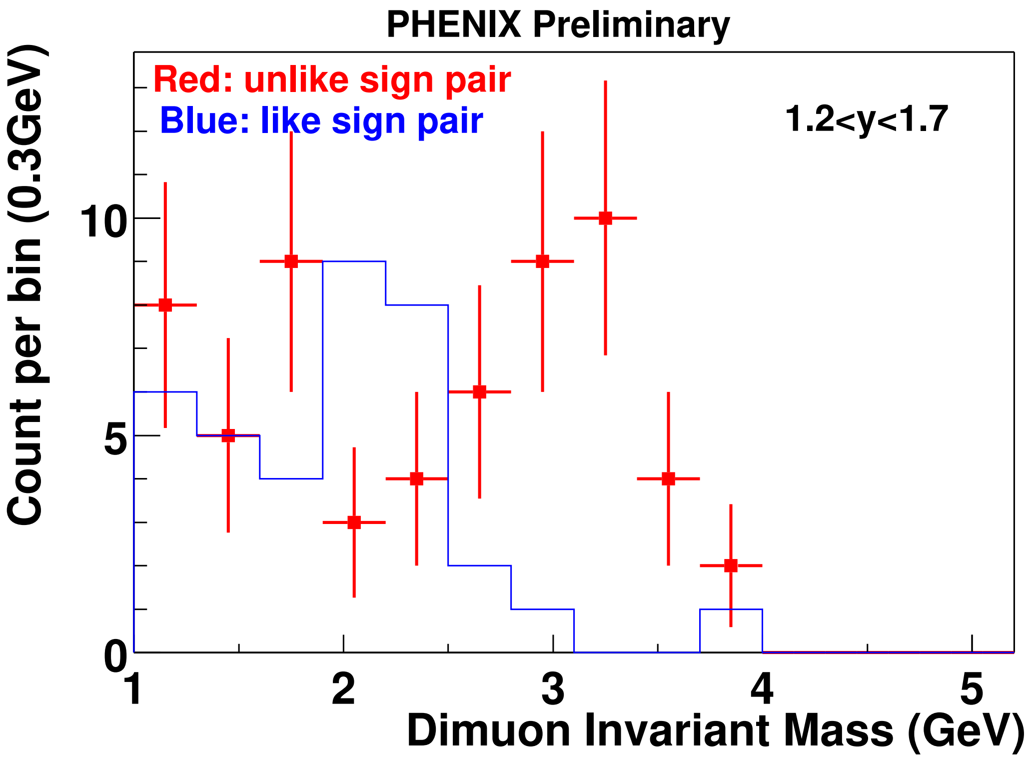

Figure 3: M_{inv} distribution for dimuons within $1.2 < y < 1.7$ passing cuts described in the text.

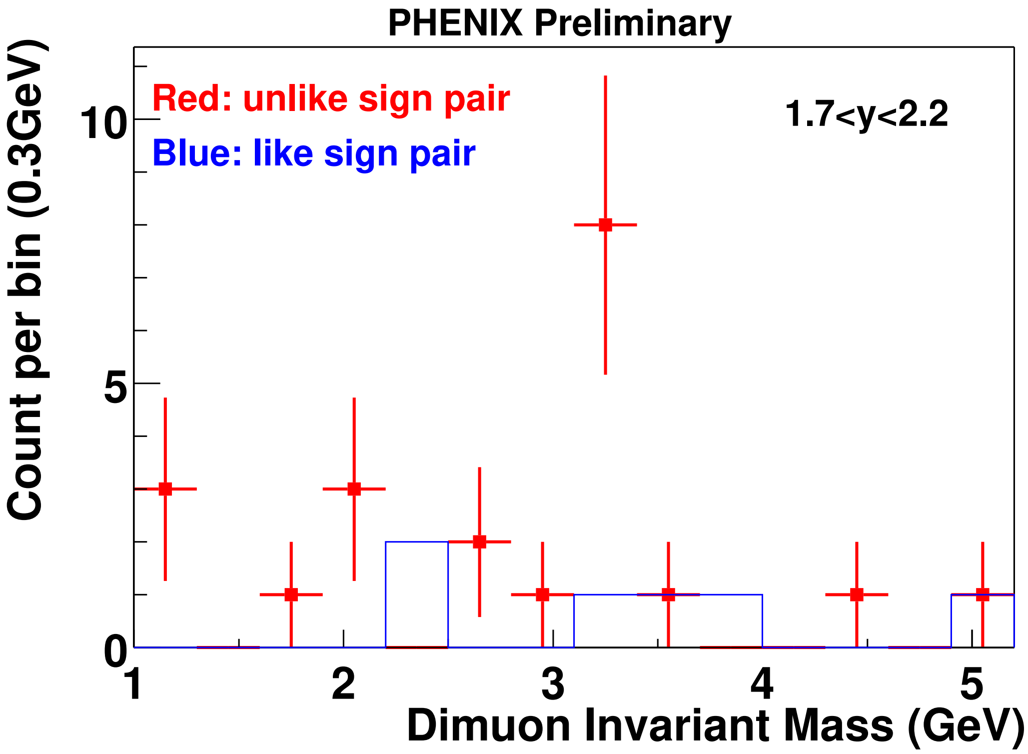

Figure 4: M_{inv} distribution for dimuons within $1.7 < y < 2.2$ passing cuts described in the text.

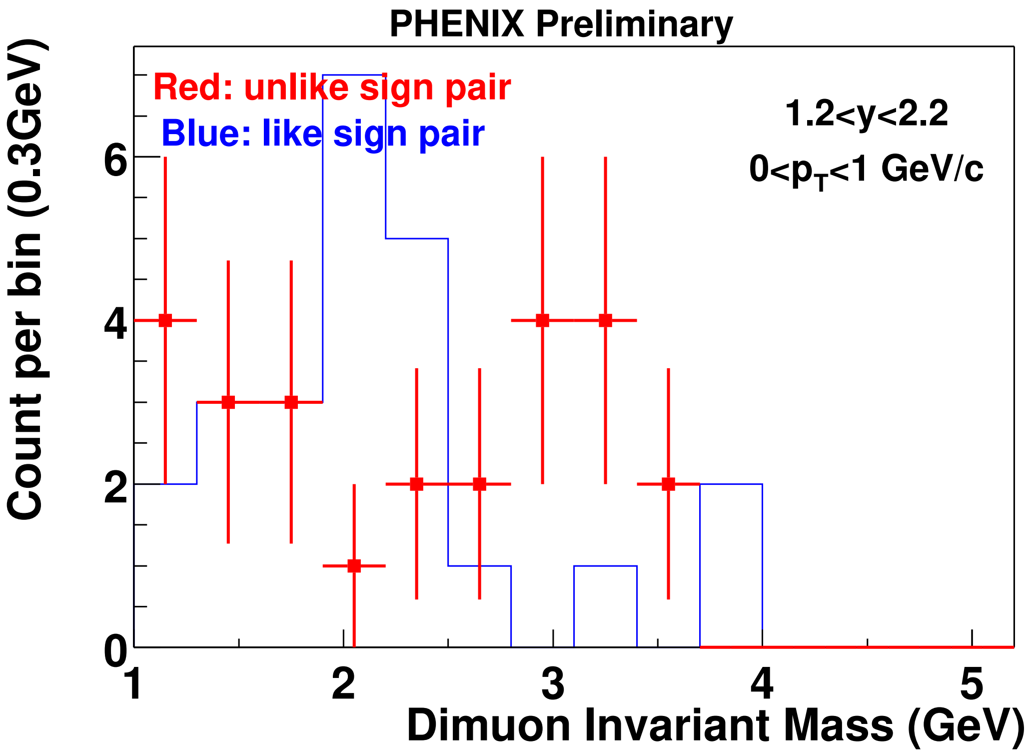

Figure 5: M_{inv} distribution for dimuons within $0 < p_{\perp}(\mathrm{GeV/c}) < 1$ passing cuts described in the text.

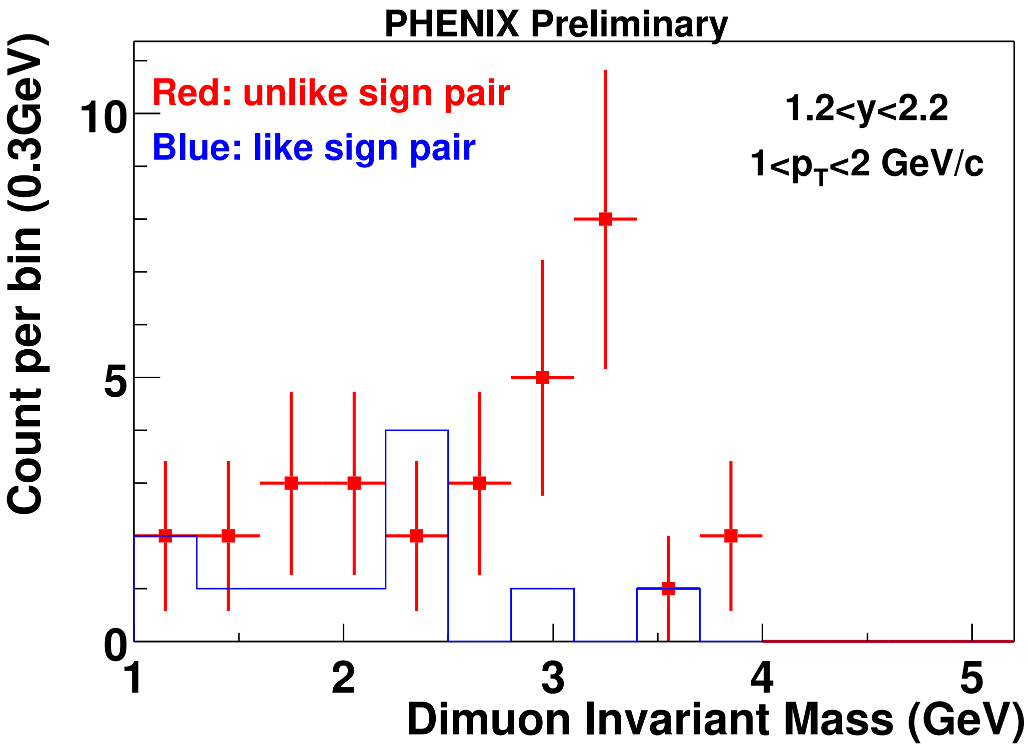

Figure 6: M_{inv} distribution for dimuons within $1 < p_{\perp}(\mathrm{GeV/c}) < 2$ passing cuts described in the text.

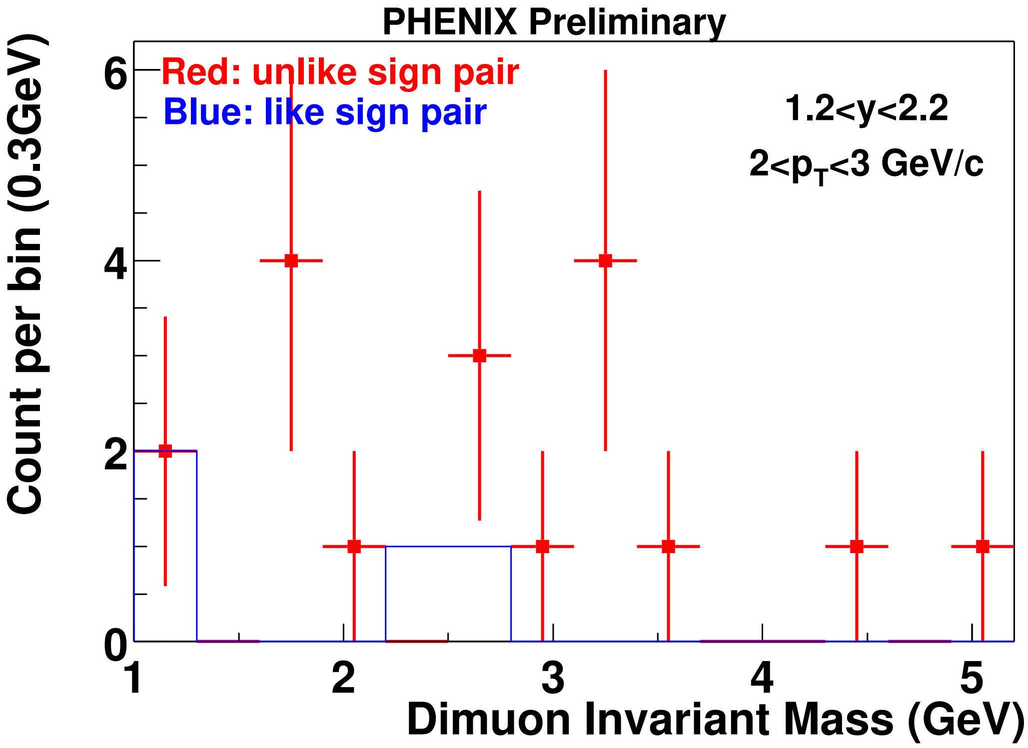

Figure 7: M_{inv} distribution for dimuons within $2 < p_{\perp}(\mathrm{GeV/c}) < 3$ passing cuts described in the text.

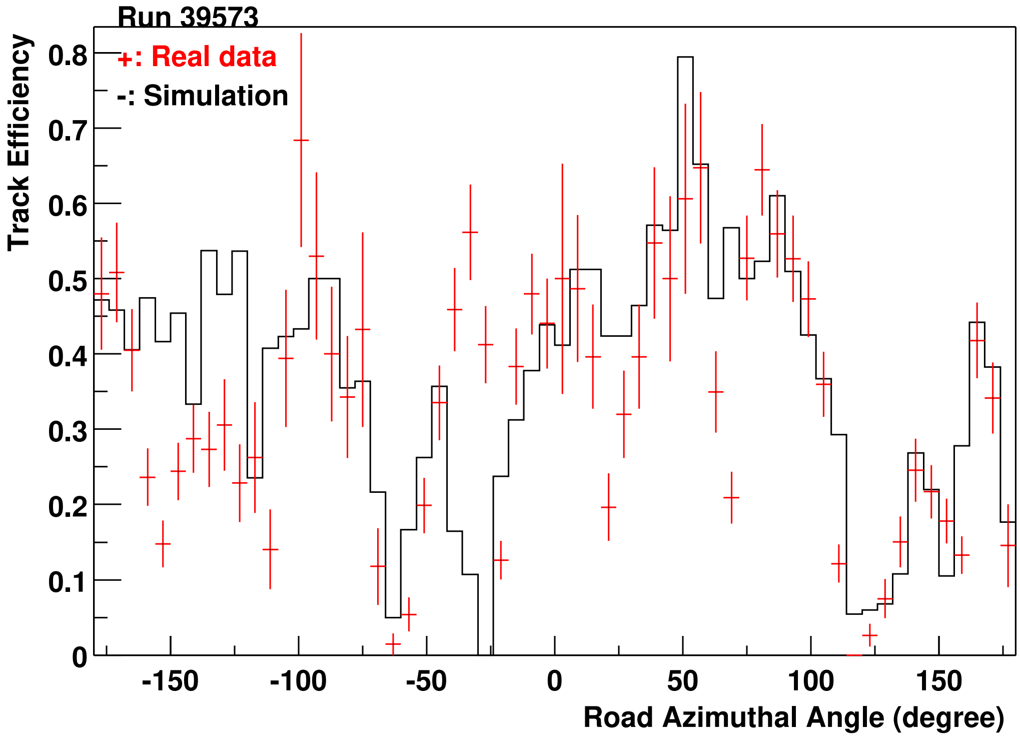

Figure 8: ϕ distribution of MuTR single-particle efficiencies (data vs. simulation).

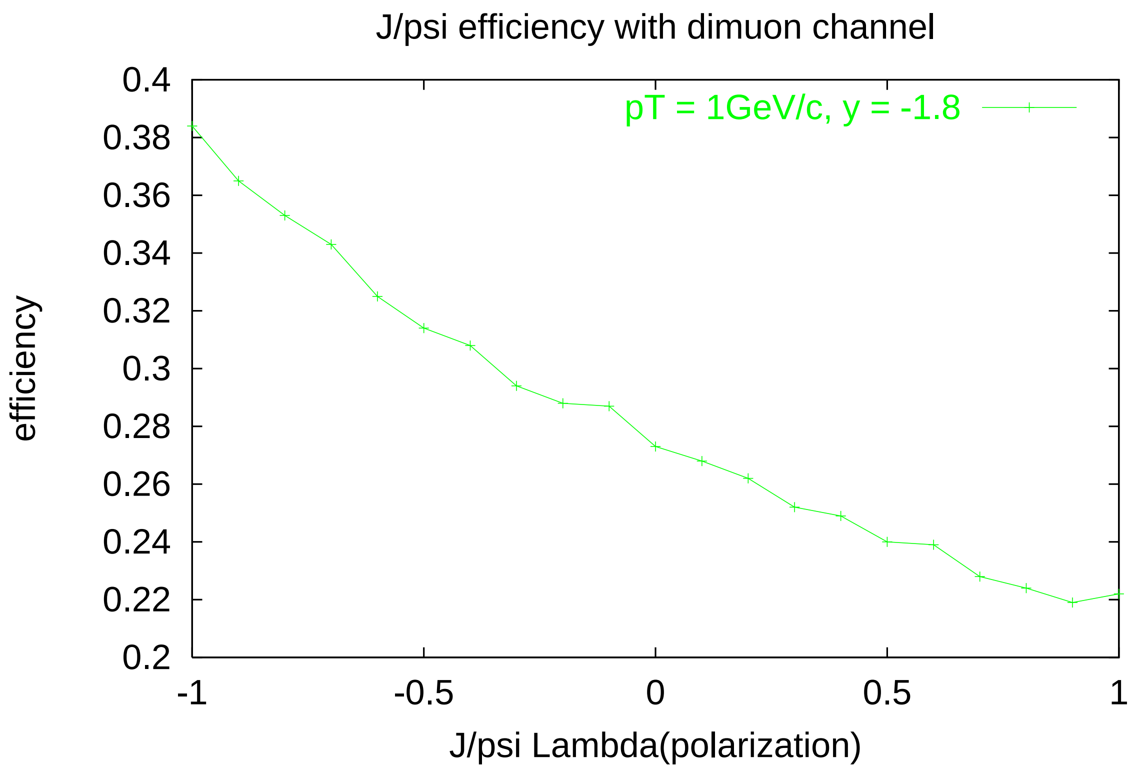

Figure 9: Jψ efficiency with the ideal South Muon Arm vs. λ (polarization parameter).

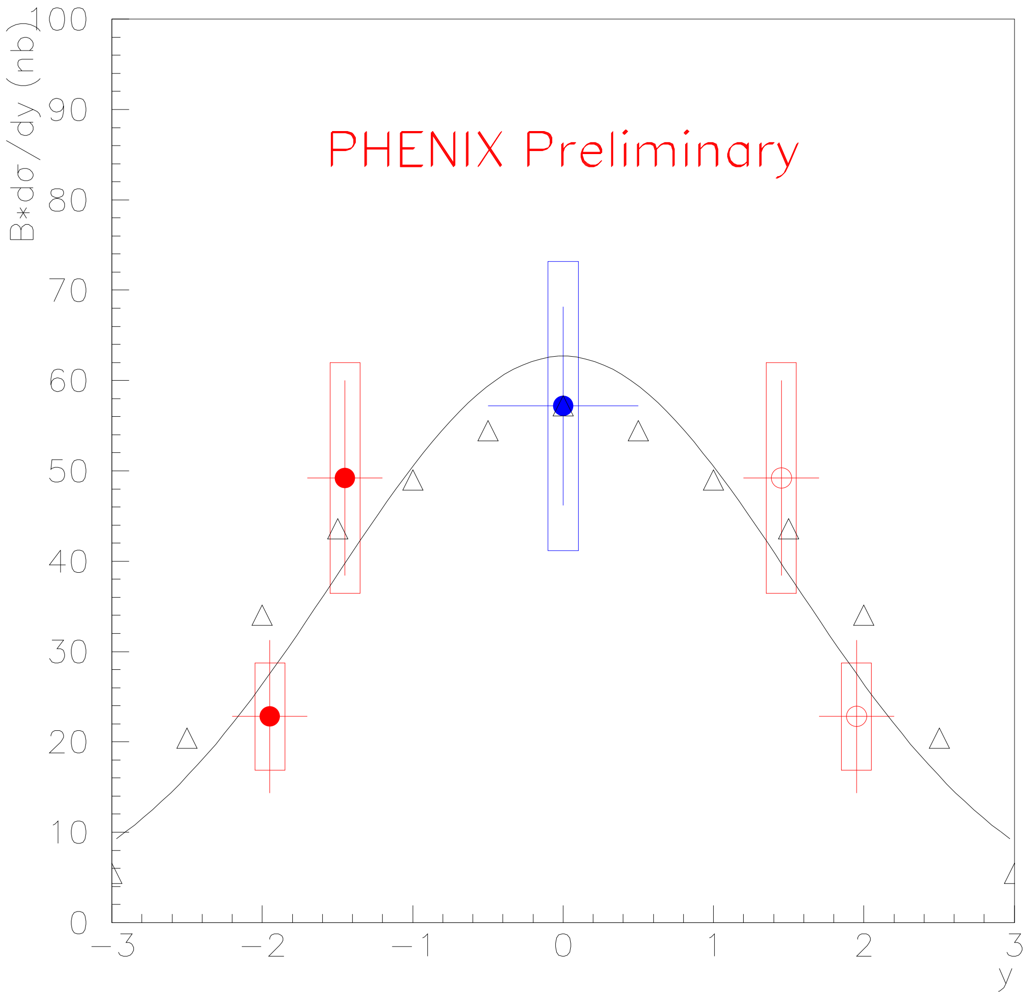

Figure 10: Rapidity distribution of $pp \rightarrow J/\Psi$ cross section from Run-2. Filled red points are from the South Muon arm. Open points are mirror images appropriate for our symmetric collisions. The blue filled point is the current central arm point. Error bars are statistical errors, boxes are systematic errors. The line is a Gaussian fit to all of the data points, giving $\sigma^{tot}_{J/\Psi} = 3980\,\mathrm{nb}$. The open triangles are pulled off by hand from the PYTHIA J/Ψ rapidity distribution Hiroki showed at last week's Heavy Flavor PWG normalized to the central arm point.

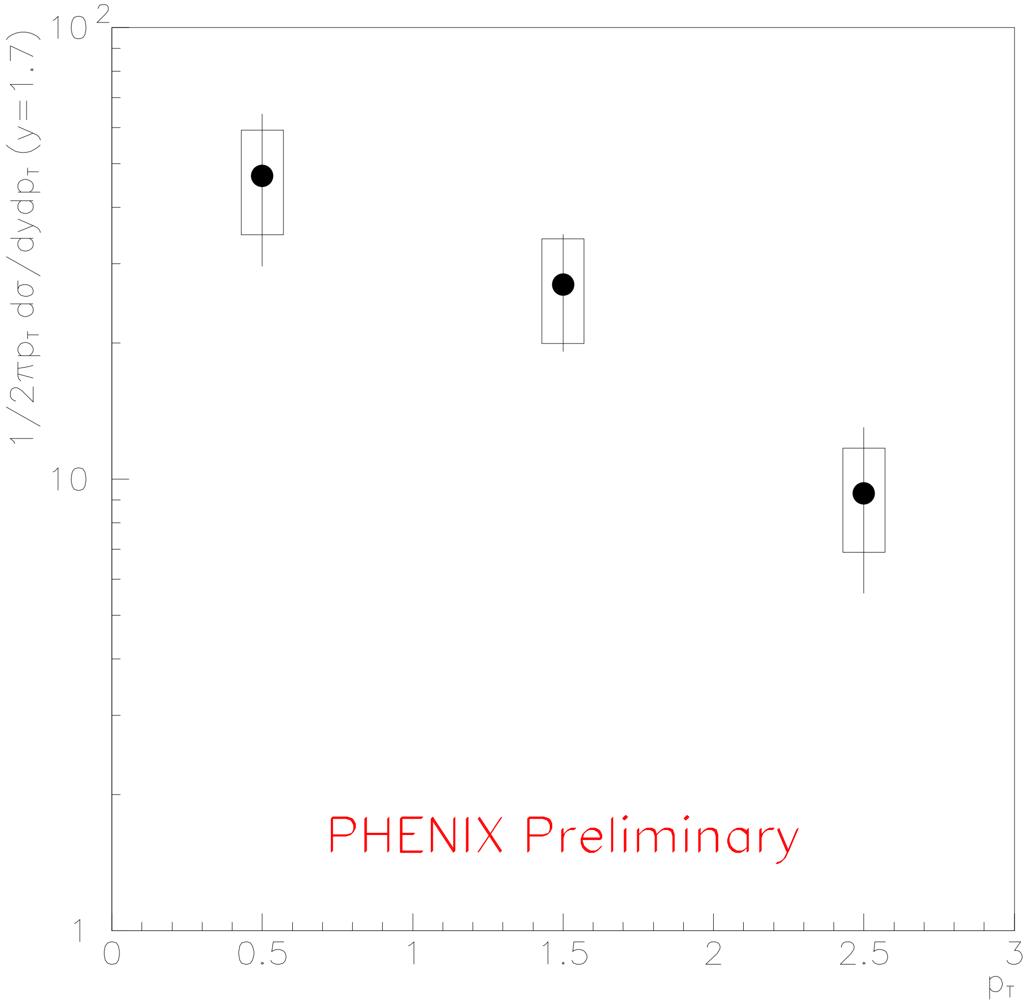

Figure 11: $p_\perp$ distribution of $pp \to J/\Psi$ cross section from Run-2. Error bars are statistical errors, boxes are systematic errors.